# Magnetic properties of low-dimensional quantum spin systems made of stable organic biradicals PNNNO, $F_2$PNNNO, and PIMNO

Yuko Hosokoshi, Yasuhiro Nakazawa, and Katsuya Inoue
*Institute for Molecular Science, Myodaiji, Okazaki, Aichi 444-8585, Japan*

Kohichi Takizawa, Hiroki Nakano, Minoru Takahashi, and Tsuneaki Goto
*Institute for Solid State Physics, University of Tokyo Roppongi, Minato-ku, Tokyo 106-8666, Japan*
(Received 10 May 1999)

Stable organic biradical crystals PNNNO, $F_2$PNNNO, and PIMNO of the PNNNO family were synthesized. {PNNNO=2-[4′- (*N*-*tert*-butyl-*N*-oxyamino)phenyl]-4,4,5,5-tetramethyl-4,5-dihydro-1*H*-imidazol-1-oxyl 3-oxide, $F_2$PNNNO=2-[2′,6′,-difluoro−4′-(*N*-*tert*-butyl-*N*-oxyamino)phenyl]- 4,4,5,5-tetramethyl-4, 5-dihydro-1*H*-imidazol-1-oxyl 3-oxide, PIMNO=2-[4′−(*N*-*tert*-butyl-*N*-oxyamino)-phenyl]-4,4,5, 5-tetramethyl-4,5-dihydro-1*H*-imidazol-1-oxyl.} PNNNO and PIMNO crystallize to form quasi-one-dimensional lattices, but $F_2$PNNNO to form a quasi-two-dimensional lattice. The temperature dependences of the susceptibility and the high-field magnetization process up to 34 T were measured down to 0.5 K. The results are analyzed by comparing with the theoretical calculations based on the crystal structures. PNNNO and PIMNO are considered to be antiferromagnetic Heisenberg spin chains consisting of $S=1/2$ spin pairs (dimers) in which the two spins are coupled ferromagnetically. At low temperatures, an antiferromagnetic ordering occurs in these crystals, which is confirmed by the thermodynamic discussion through specific heat measurements. On the other hand, $F_2$PNNNO is thought to be a two-dimensional Heisenberg system, in which the spin pairs are connected by two types of antiferromagnetic interactions. The ground state is singlet. The high-field magnetization process shows a two-step saturation with a plateau of the half value of the saturation magnetization. [S0163-1829(99)00342-2]

## I. INTRODUCTION

The study of quantum spin systems has attracted much attention for several decades. According to Haldane's conjecture in 1983, different ground states are expected for the antiferromagnetic chain systems of integer and half-odd-integer spins.[1] Experimental study on the $S=1/2$ and $S=1$ system have been reported for several compounds of $Cu^{2+}$ and $Ni^{2+}$, respectively, and the existence of an energy gap in the $S=1$ antiferromagnetic chain system was confirmed for a $Ni^{2+}$ compound $[NENP=Ni(C_2H_8N_2)_2NO_2(ClO_4)]$.[2] The intermediate states between the $S=1/2$ and $S=1$ antiferromagnetic chains are now an attractive problem. The theoretical[3] and experimental[4–6] studies on the $S=1/2$ ferromagnetic and antiferromagnetic alternating chain have been reported. The reported compounds are Cu compounds[4,5] and an organic monoradical.[6] In these compounds, the ratio of the exchange coupling $\alpha=J_F/|J_{AF}|$ is at most about two, where $J_F$ and $J_{AF}$ represent ferro- and antiferromagnetic exchange couplings, respectively.

In this article, we report on the magnetic properties of the antiferromagnetic lattice of $S=1/2$ spin pairs in which the two spins are strongly coupled ferromagnetically. We designed stable organic biradicals, in which two $S=1/2$ spins coupled ferromagnetically with $2J_F/k_B=216-638$ K. By attributing the ferro- and antiferromagnetic exchange couplings to the intra- and intermolecular ones, we have successfully obtained the spin systems with a large $\alpha$ (=6, 18, 44).

We have recently found that an organic biradical of PNNNO has a large intramolecular ferromagnetic exchange coupling,[7] where PNNNO=2-[4′-(*N*-*tert*-butyl-*N*-oxyamino)phenyl]-4, 4, 5, 5-tetramethyl-4,5-dihydro-1*H*-imidazol-1-oxyl 3-oxide. We synthesize two related biradicals of $F_2$ PNNNO and PIMNO and observe the change of the magnitude of the intramolecular exchange couplings, where $F_2$PNNNO=2-[2′,6′,-difluoro-4'-(*N*-*tert*-butyl-*N*-oxyamino)phenyl]-4, 4, 5, 5-tetramethyl-4, 5-dihydro-1*H*-imidazol-1-oxyl 3-oxide, and PIMNO=2-[4'-(*N*-*tert*-butyl-*N*-oxyamino)phenyl]-4,4,5,5-tetramethyl-4,5-dihydro-1*H*-imidazol-1-oxyl.[8,9] The molecular structures of these biradicals are shown in Fig. 1.

The characteristics of the PNNNO family are excellent stability and crystallinity, tuning of the intramolecular ferromagnetic exchange coupling by the chemical modification,[9] and the existence of the weak intermolecular antiferromagnetic interactions in addition to the large intramolecuar interactions in the crystals.

The PNNNO family includes two $S=1/2$ spins, which are mainly distributed on the NO groups marked by the ellipses in Fig. 1. The ellipses correspond to the molecular orbital of unpaired electrons, i.e., a singly occupied molecular orbital (SOMO). An $S=1/2$ spin mainly concentrates on an NO

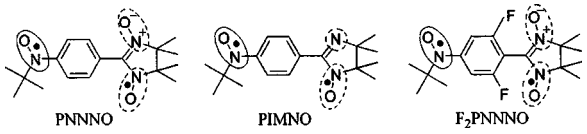


FIG. 1. Molecular structures of the compounds studied here. Ellipses represent a molecular orbital of unpaired electrons.

 

group within an ellipse of a solid curve, and the other on the NO groups within ellipses of a broken curve. Hereafter, we distinguish these radical units in PNNNO and $F_2$PNNNO as *t*Bu-NO (corresponding to *N-tert*-butyl nitroxide) and NN (corresponding to nitronyl nitroxide) units, respectively. The two NO groups in the NN skeleton are equivalent to each other. The removal of the oxygen atom of the NN unit in PNNNO yields PIMNO. We call the radical unit of the broken ellipses in PIMNO as IN (corresponding to imino nitroxide) unit.

The sign of the intramolecular exchange coupling between two radical units is understood by the spin polarization effect. The bonding scheme of the two radical units in the PNNNO family brings about a ferromagnetic exchange coupling between the *t*Bu-NO and NN (IN) units.

The intermolecular exchange interaction in organic crystals is governed by the overlap between the molecular orbitals. Especially the antiferromagnetic exchange couplings are brought about by the overlap between SOMO's.[10] As mentioned above, the SOMO of the PNNNO family is distributed mainly on the NO groups. Therefore, intermolecular antiferromagnetic interactions are expected for the contacts between the NO groups. We must mention that the nitrogen and oxygen atoms in the NO groups have partially positive and negative charges, respectively. In the neutral organic molecular crystals, the crystal structures are always dominated by the electrostatic energies. The close spacing between the NO groups is preferable in the electrostatic aspects, and such contacts are sometimes observed in the NN derivatives.[10]

Therefore, the PNNNO family is an attractive magnetic system with ferro- and antiferromagnetic interactions. The magnetic properties of PNNNO, $F_2$PNNNO, and PIMNO are investigated and discussed on the basis of the crystal structures. The crystal structures of PNNNO and $F_2$PNNNO are similar to each other: both include uniform chains constructed by the contacts between the NN units. For biradicals, two types of uniform chain structures are possible, which are shown in Fig. 2. PNNNO and $F_2$PNNNO involve the chain of type I and PIMNO includes the one of type II. In the extreme limit of $J_F \to \infty$, both models become equivalent to the antiferromagnetic uniform chain of $S=1$. However, in the limit of $J_F \to 0$, type I and II become the antiferromagnetic uniform chain of $S=1/2$ and isolated dimer model, respectively. For type II, the numerical calculation has already been reported for the case of $J_F/|J_{AF}| \leqslant 8$.[11] We perform the numerical calculations for both models with the wider range of $J_F/|J_{AF}|$ to analyze our experimental results. Among the three compounds, only $F_2$PNNNO has an energy gap above the singlet ground state. The temperature dependence of the paramagnetic susceptibilities ($\chi_p$) decreases exponentially to zero as $T \to 0$. The characteristic of $F_2$PNNNO is seen in the high-field magnetization. The high-field magnetization process shows a two-step saturation of which intermediate plateau corresponding to the half value of the saturation magnetization. Our theoretical treatments reveal that the interchain interactions play an important role on the appearance of the plateau. This is a rare example of the observation of the plateau in a magnetization curve in a two-dimensional system. The other two compounds undergo antiferromagnetic phase transitions due to the weak interchain interactions, which are confirmed by the heat capacity measurements.

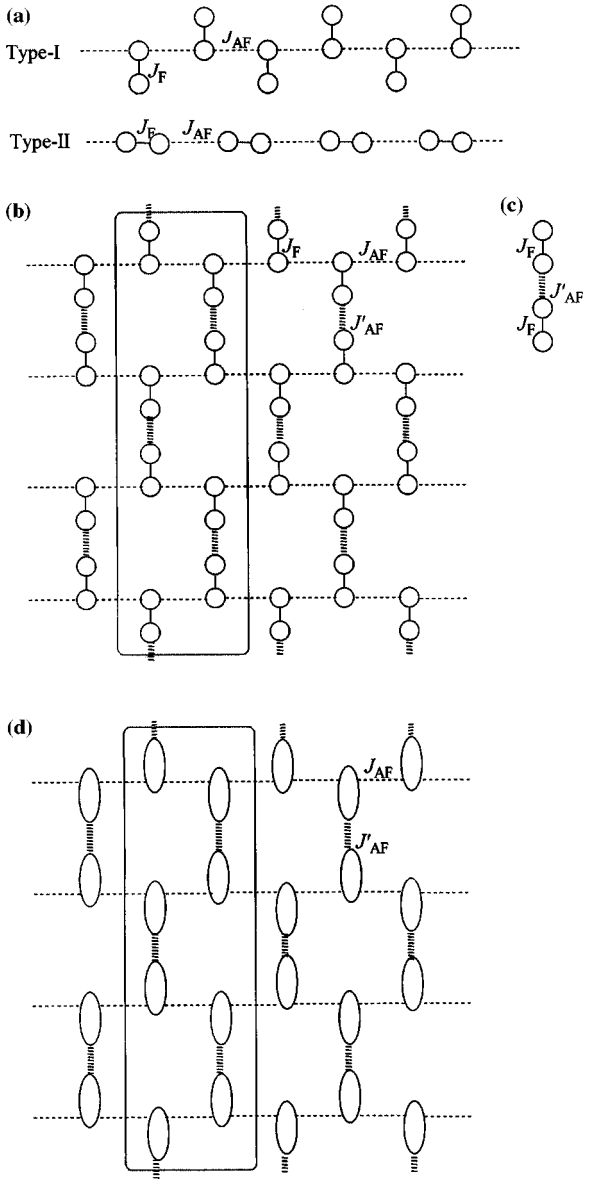


FIG. 2. Schematic illustration of the magnetic interaction networks studied in this work. (a) Two types of uniform chains with intramolecular ferromagnetic coupling ($2J_F$) and intrachain antiferromagnetic coupling ($2J_{AF}$). Type I: the model of PNNNO, Type II: the model of PIMNO. (b) Type-I chain with interchain antiferromagnetic interactions ($J'_{AF}$). The magnetic model for $F_2$PNNNO. (c) Isolated 4-spin model with $S=1/2$. The extreme limit of the model (b) when $J_{AF} \to 0$. (d) Antiferromagnetic honeycomb lattice with $S=1$. The extreme limit of the model (b) when $J_F \to \infty$.

## II. EXPERIMENT

The materials PNNNO, $F_2$PNNNO, and PIMNO are synthesized by following the method described in the literatures[7,9] and purified by the recrystallization from concentrated solutions.

Static magnetic susceptibilities were measured using a quantum design MPMS 5S superconducting quantum interference device magnetometer in the temperature range of 1.8–350 K for the randomly oriented crystals. The magneti-

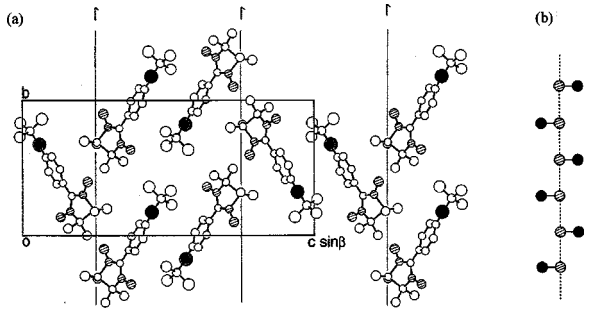


FIG. 3. (a) Crystal structure of PNNNO viewed along the *a* axis. Black and shaded ellipses represents the NO groups of *t*Bu-NO and NN units, respectively. $P2_1/n$, $a=6.155$, $b=11.356$, $c=24.995$ Å, $\beta=96.48°$, $V=1735.8$ Å$^3$, $Z=4$. (b) Schematic display of the crystal structure of PNNNO. Black and shaded circles correspond to the *t*Bu-NO and NN units, respectively. Solid and broken lines represent the exchange path of the intra- and intermolecular interactions, respectively.

zation processes for microcrystalline samples down to 0.5 K were measured using a $^3$He cryostat in static fields up to 17 T produced by a superconducting magnet with a sample-extraction method or in pulsed magnetic fields up to 40 T of a duration time of about 10 ms produced by a wire-wound pulse magnet. The specific heat was measured by the thermal relaxation technique in a $^3$He cryostat in the temperature region between 0.7 and 4.5 K.

## III. CRYSTAL STRUCTURES

### A. PNNNO and $F_2$PNNNO

The crystals of PNNNO belong to the monoclinic system, space group $P2_1/n$, with $a=6.155(2)$, $b=11.356(2)$, $c=24.995(6)$ Å, $\beta=96.48(2)°$, $V=1735.8(7)$ Å$^3$, and $Z=4$.[7] The crystal system of $F_2$PNNNO is the orthorhombic system, space group $Pbca$, with $a=19.807(4)$, $b=13.985(4)$, $c=13.456(3)$ Å, $V=3727(2)$ Å$^3$, and $Z=8$. The crystal structures of PNNNO and $F_2$PNNNO are compared in Figs. 3(a) and 3(b) and Figs. 4(a) and 4(b). In both

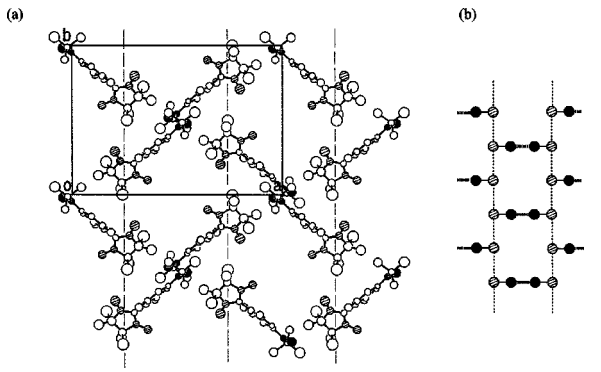


FIG. 4. (a) Crystal structure of $F_2$PNNNO projected on the *ab* plane. $Pbca$, $a=19.857$, $b=14.010$, $c=13.481$ Å, $V=3750.5$ Å$^3$, $Z=8$. Black and shaded ellipses represent the NO groups of *t*Bu-NO and NN units, respectively. (b) Schematic display of the crystal structure of $F_2$PNNNO. Black and shaded circles correspond to the *t*Bu-NO and NN units, respectively. Solid and broken lines represent the exchange path of the intra- and intermolecular interactions, respectively.

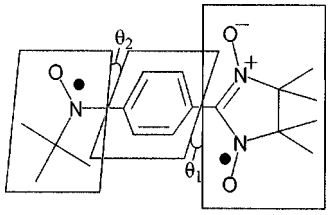


FIG. 5. Two kinds of dihedral angles in PNNNO skeleton.

cases, noticeable is the uniform chain along the *b* axis. The close spacing between the NN units is commonly observed. The PNNNO molecules related by the twofold screw symmetry have the contacts with the interatomic distances of 4.988 and 5.230 Å between the nitrogen and oxygen atoms. The $F_2$PNNNO molecules related by the *b*-glide reflection symmetry have the contact with the interatomic distance of 4.981(6) Å between the oxygen atoms.

In contrast with the similar chain structures, molecular packing between chains are different from each other. The packing between the molecules connected by an inversion symmetry is different. In the crystals of $F_2$PNNNO, noticeable is the short contact [3.878(8) Å] between the oxygen atoms of the *t*Bu-NO's related by an inversion symmetry. On the other hand, the *t*Bu-NO's of the PNNNO molecule are separated with the distance of 4.896 Å between the nitrogen and oxygen atoms.

The different interchain molecular arrangements are related to the difference in the molecular structures. There is noticeable difference in the dihedral angles between the benzene ring and radical planes. We define $\theta_1$ and $\theta_2$ as the dihedral angles between the benzene ring and the NN plane or *t*Bu-NO plane, respectively (Fig. 5). The molecule of $F_2$PNNNO has large $\theta_1$ (53.8°) and small $\theta_2$ (2.2°), whereas the one of PNNNO takes 25° and 22°, respectively. The origin of the large $\theta_1$ in $F_2$PNNNO is explained by the electrostatic repulsion between the oxygen atom of the NN unit and the fluorine atom of the benzene ring. Noticeable is the strong relationship between the small $\theta_2$ and the short contact of *t*Bu-NO's in $F_2$PNNNO.

The magnetic model of PNNNO is represented by the type-I chain in Fig. 2(a) by the consideration of the intramolecular ferromagnetic coupling and the antiferromagnetic coupling between the NN units along the *b* axis. In the case of $F_2$PNNNO, the interchain interactions produced by the contact of *t*Bu-NO's yield the two-dimensional model shown in Fig 2(b).

### B. PIMNO

The crystals of PIMNO belong to the monoclinic system, space group $P2_1$, with $a=6.225(2)$, $b=10.499(3)$, $c=13.029(2)$ Å, $\beta=94.37(2)°$, $V=848.7(3)$ Å$^3$, and $Z=2$. The crystal structure of PIMNO projected on the *bc* plane is shown in Fig. 6. Noticeable is the close spacing between the *t*Bu-NO and imino nitroxide (IN) to form a uniform chain with the interatomic distance of N···O 4.588(8) Å between the molecules related by the translation symmetry along the *b* axis. The magnetic model of PIMNO can be expressed by the type-II chain in Fig. 2(a) on

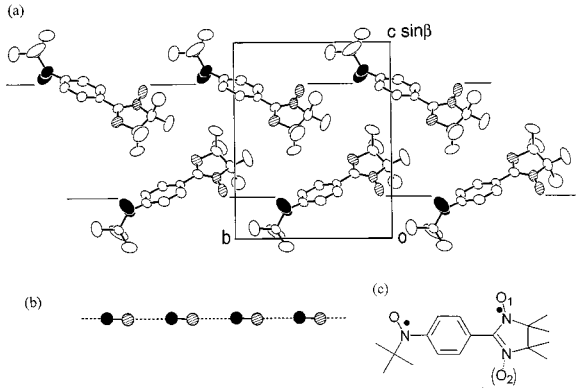


FIG. 6. (a) Crystal structure of PIMNO viewed along the $c$ axis. $P2_1$, $a=6.277$, $b=10.495$, $c=13.036$ Å, $\beta=94.37°$, $V=849.5$ Å$^3$, $Z=2$. Black and shaded ellipses represent the NO groups of $t$Bu-NO and IN units, respectively. (b) Schematic display of the crystal structure of PIMNO. Black and shaded circles correspond to the $t$Bu-NO and IN units, respectively. Solid and broken lines represent the exchange path of the intra- and intermolecular interactions, respectively. (c) Disorder of the site of the oxygen atom in PIMNO. (see text)

the assumption of the intramolecular ferromagnetic coupling and the antiferromagnetic coupling between the $t$Bu-NO and IN units.

## IV. THEORETICAL TREATMENTS OF THE SPIN CHAINS OF TYPE I AND II

The Hamiltonian of the type-I Heisenberg chain in Fig. 2(a) is described by

$$\mathcal{H}=-2J_{\mathrm{AF}}\sum_{i}^{N/2}(\boldsymbol{S}_{2i-1}\cdot\boldsymbol{S}_{2i+1}-\alpha\boldsymbol{S}_{2i-1}\cdot\boldsymbol{S}_{2i}). \quad (4.1)$$

The Hamiltonian of the type-II chain in Fig. 2(a) is written as

$$\mathcal{H}=-2J_{\mathrm{AF}}\sum_{i}^{N/2}(\boldsymbol{S}_{2i}\cdot\boldsymbol{S}_{2i+1}-\alpha\boldsymbol{S}_{2i}\cdot\boldsymbol{S}_{2i-1}), \quad (4.2)$$

where $S$ denotes the $S=1/2$ spin operator and $N$ is the number of sites, which should be even. We define $\alpha=J_{\mathrm{F}}/|J_{\mathrm{AF}}|$. For these models, we perform exact diagonalizations of a chain with even length up to 14 spins and calculate the susceptibility. Numerical studies of the type-II chain at finite temperatures were reported only for $\alpha\leqslant 8$.[11] Since PIMNO corresponds to the type-II chain with $\alpha>8$, we perform the calculations for $\alpha$ with wider range. We find that the deviation between the susceptibility curves for 14-spin and 12-spin uniform chains is within 1% for $k_{\mathrm{B}}T/|2J_{\mathrm{AF}}|\geqslant 0.4$. Therefore, we use the curves for 14 spins at $k_{\mathrm{B}}T/|2J_{\mathrm{AF}}|\geqslant 0.4$ as an approximation for infinite spins. It is worth mentioning that, both models of type I and II for the same $\alpha$ yield indistinguishable curves in the above-temperature range, in spite of the fact that the ground states of these models are expected to be different from each other.

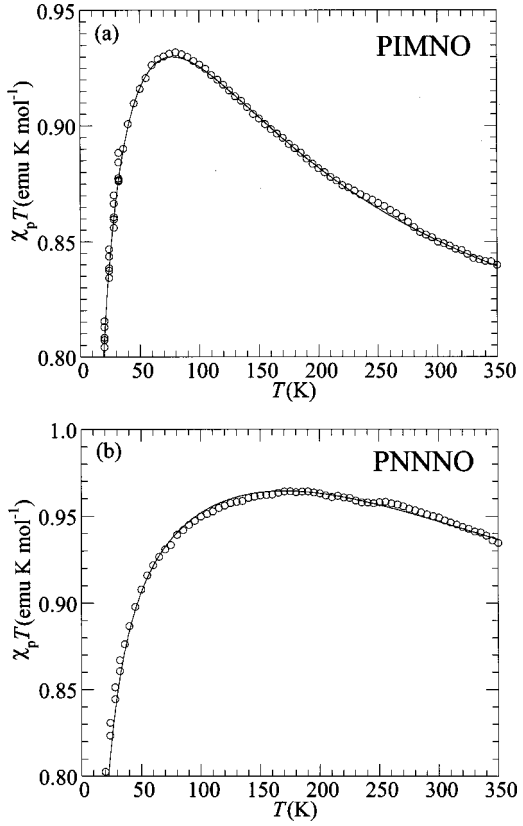


FIG. 7. (a) Temperature dependence of $\chi_{\mathrm{p}}T$ of PIMNO. (b) Temperature dependence of $\chi_{\mathrm{p}}T$ of PNNNO.

## V. MAGNETIC AND THERMODYNAMIC PROPERTIES OF PIMNO AND PNNNO

The temperature dependences of $\chi_{\mathrm{p}}$'s of PIMNO and PNNNO are shown in Fig. 7, where the values of $\chi_{\mathrm{p}}T$ are plotted as a function of $T$. We analyze these experimental results based on the theoretical models described in the previous section. The susceptibilities of the type-I and -II chains as a function of $k_{\mathrm{B}}T/|2J_{\mathrm{AF}}|$ for various $\alpha$ at an interval of one are calculated. Using these, we adjust the value of $2J_{\mathrm{AF}}/k_{\mathrm{B}}$ in order to fit the observed data. This fitting procedure includes at most 1% ambiguity in the estimation of the values of $J_{\mathrm{AF}}$ and $J_{\mathrm{F}}$. This uncertainty is small enough in comparison to the experimental error. The calculated results for the parameter set of $2J_{\mathrm{F}}/k_{\mathrm{B}}=216$ K and $2J_{\mathrm{AF}}/k_{\mathrm{B}}=-12$ K reproduces well the experimental results of PIMNO. The calculation with $2J_{\mathrm{F}}/k_{\mathrm{B}}=638$ K and $2J_{\mathrm{AF}}/k_{\mathrm{B}}=-14.5$ K also satisfactorily fits the experiments of PNNNO. The solid curves in Fig. 7 represent the calculations with the above parameters.

In the low-temperature region, $\chi_{\mathrm{p}}$'s show broad maxima at around 3 K in PIMNO and 2 K in PNNNO. Figure 8(a) shows the temperature dependence of the $M/B$ ratios of PIMNO under various applied fields. It is obvious that the linear field dependence is lost below 2.5 K. This behavior corresponds to the spin flop when the material undergoes an antiferromagnetic ordering. The magnetization isotherm at the lowest temperature (0.5 K) exhibits an upturn above 0.2 T, corresponding to the spin flop. [Fig. 8(b)] These behaviors suggest the antiferromagnetic phase transition occurs at 2.5 K.

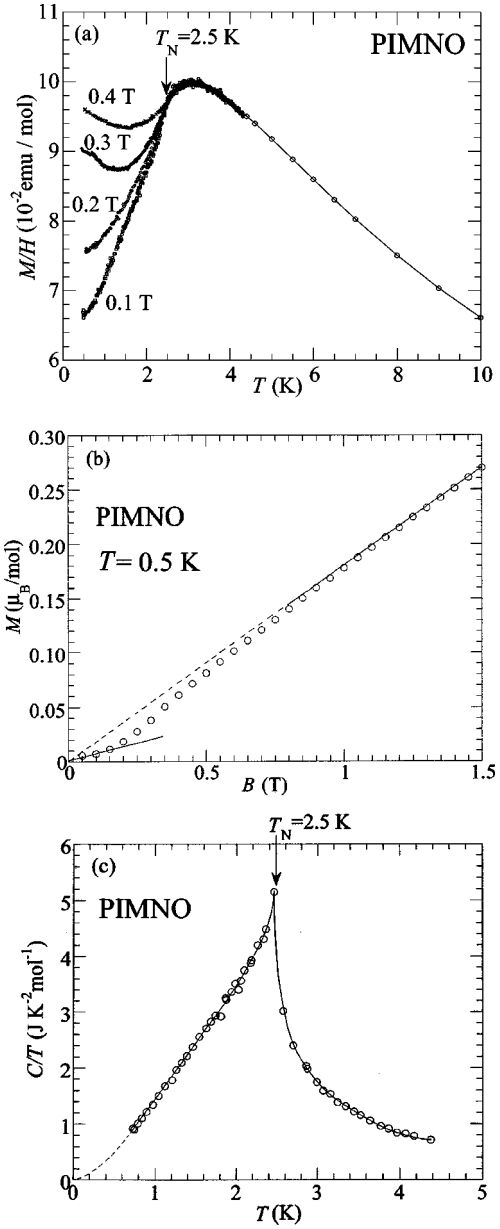


FIG. 8. (a) Temperature dependence of $M/B$ of PIMNO measured under various applied fields. (b) Magnetization isotherm of PIMNO at 0.5 K below 1.5 T. (c) Temperature dependence of heat capacity of PIMNO plotted as a function of $C/T$.

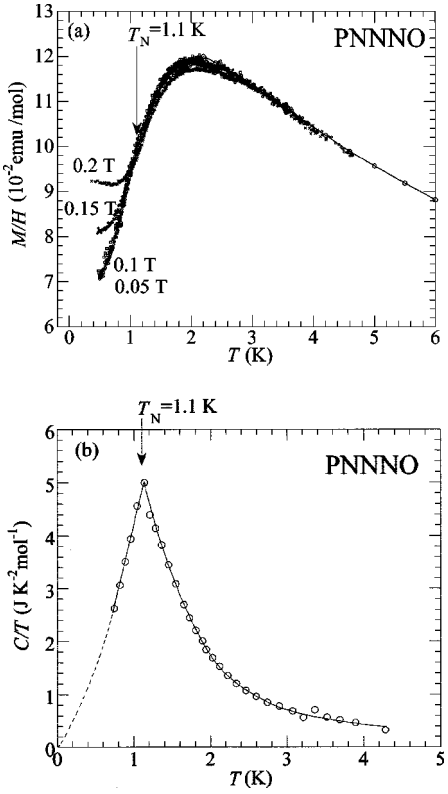


FIG. 9. (a) Temperature dependence of $M/B$ of PNNNO measured under various applied fields. (b) Temperature dependence of heat capacity of PNNNO plotted as a function of $C/T$.

The three-dimensional phase transition is furthermore examined by the heat capacity measurements. Figure 8(c) shows the temperature dependence of the heat capacity of PIMNO. The λ-shaped peak was observed at 2.5 K. This also indicates that antiferromagnetic ordering appears at 2.5 K. The open circles plotted are the raw data without the subtraction of the lattice contribution, which is small in this temperature region, on the assumption of the Debye temperature of about 90–140 K reported for the organic radical having similar chemical structure.[12] The lattice contribution at 3 K is at most 3% and decreases with a function of $T^{-3}$. Therefore, the lattice contribution is negligibly small and does not affect our following discussion.

The magnetic entropy change ($\Delta S$) obtained by the integration of $C/T$ with $T$ between 0.7∼4.5 K is 7.5 $\mathrm{J\,K^{-1}\ mol^{-1}}$. Assuming that the lower-temperature range below 0.7 K gives the value of $\Delta S \simeq 0.2 \sim 0.3 \mathrm{J\,K^{-1}\ mol^{-1}}$ by the simple extrapolation to $T \rightarrow 0$ based on the spin-wave model, the total magnetic entropy at 4.5 K is estimated at about 7.8 $\mathrm{J\,K^{-1}\ mol^{-1}}$. In general, the total magnetic entropy ($S_{\mathrm{tot}}$) at $T \rightarrow \infty$ for $N$ spins of the spin value of $s$ approaches $Nk_{\mathrm{B}} \ln(2s+1)$. In the present case, each molecule includes two $S=1/2$ spins, and $S_{\mathrm{tot}}$ should approach $2N_{\mathrm{A}}k_{\mathrm{B}} \ln 2$ ($=11.5$ $\mathrm{J\,K^{-1}\ mol^{-1}}$) at $T \rightarrow \infty$. If we take into account that $J_{\mathrm{F}}$ is more than ten times larger than $|J_{\mathrm{AF}}|$ in PIMNO, it is expected that, at $k_{\mathrm{B}}T \leqslant |2J_{\mathrm{AF}}|$, two $S=1/2$ spins within each molecule are strongly coupled ferromagnetically to form an $S=1$ species. Then, we can expect the magnetic entropy of $N_{\mathrm{A}}k_{\mathrm{B}} \ln 3$ ($=9.13$ $\mathrm{J\,K^{-1}\ mol^{-1}}$) toward $T \simeq |2J_{\mathrm{AF}}|/k_{\mathrm{B}}$. The magnetic entropy of PIMNO at 4.5 K is estimated to be about 7.8 $\mathrm{J\,K^{-1}\ mol^{-1}}$, which corresponds to 85% of $N_{\mathrm{A}}k_{\mathrm{B}} \ln 3$. This behavior agrees well with the expectation of the existence of 1 mol of $S=1$ species, which are coupled antiferromagnetically to one another at $T \leqslant |2J_{\mathrm{AF}}|/k_{\mathrm{B}}$. The slow saturation toward $N_{\mathrm{A}}k_{\mathrm{B}} \ln 3$ suggests the low-dimensional nature of this material. Therefore, we conclude that PIMNO undergoes an antiferromagnetic ordering at 2.5 K.

In the case of PNNNO, an antiferromagnetic ordering is also observed at 1.1 K. The spin flop related to the antiferromagnetic ordering is found in the magnetic measurements. A nonlinear field dependence appears below about 1 K in the temperature variation of the magnetization with various applied fields. [Fig. 9(a)] The magnetization isotherm at the lowest temperature (0.5 K), which is very similar to that of

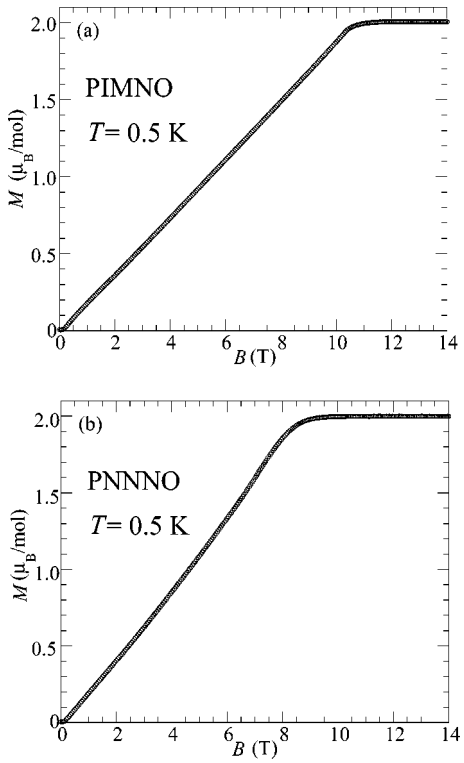


FIG. 10. (a) Magnetization isotherm of PIMNO at 0.5 K up to 14 T. (b) Magnetization isotherm of PNNNO at 0.5 K up to 14 T.

PIMNO, has an anomaly at about 0.12 T, corresponding to the spin flop. The temperature dependence of the heat capacity exhibits a λ-shaped peak at 1.1 K. The entropy gained within the experimental temperature range (0.7∼4.5 K) is estimated to be 6.0 $\mathrm{J\,K^{-1}\ mol^{-1}}$. The extrapolation to $T=0$ adds $\Delta S$ by 0.6∼0.7 $\mathrm{J\,K^{-1}\ mol^{-1}}$ and the total entropy at 4.5 K is estimated to be 6.7 $\mathrm{J\,K^{-1}\ mol^{-1}}$, which corresponds to 73% of $N_A k_B \ln 3$. This behavior is the evidence of the antiferromagnetic phase transition of PNNNO at 1.1 K.

The magnetization isotherms of PIMNO and PNNNO at 0.5 K are shown in Fig. 10. The values of the magnetization of both compounds increase linearly and reach the saturation moment for parallel-aligned $S=1$ species (2 $\mu_B$ $\mathrm{mol^{-1}}$), whereas an ideal one-dimensional compound is expected to show the field dependence with a concave shape. We consider that the linear field dependence of each material reflects the influence of the interchain interactions, since the system is in the three-dimensional antiferromagnetic ordering in this temperature region.

From the saturation field ($B_{sat}$), we can roughly estimate the antiferromagnetic exchange couplings. On the assumption of the antiferromagnetic uniform chains of $S=1$, we can estimate $2J/k_B=-14.1$ and $-11.4$ K from $B_{sat}=10.5$ and 8.5 T for PIMNO and PNNNO, respectively. For PIMNO, the value of $J$ is slightly larger than the one obtained from the susceptibility ($2J_{AF}=-12$ K). The large value reflects the contribution of interchain antiferromagnetic interactions. On the other hand, for PNNNO, the estimated value is smaller than the one from the susceptibility ($2J_{AF}=-14.5$ K). The reason is not clear, but the existence of the ferromagnetic contribution in the interchain interactions is suspected.

In the crystals of PIMNO, the oxygen site of the imino nitroxide unit is disordered; the probability of the occupancy of the O1 and O2 sites are 64.1(6) and 35.8(7) %, respectively. [Fig. 6(c)] We can see the close spacing between the O2 site and the *t*Bu-NO along the *a* and *c* directions with the interatomic distances of about 5 Å . These interchain interactions result in the antiferromagnetic order at 2.5 K. On the other hand, the chains in PNNNO are considerably separated. Between the molecules related by an inversion symmetry, we can notice the short distance of 4.89 Å between the N and O atoms in the *t*Bu-NO's. Other interatomic distances are longer than 6 Å . This is the reason for the lower $T_N$ of PNNNO than the one of PIMNO.

## VI. MAGNETIC PROPERTIES OF $F_2$PNNNO

The temperature dependence of $\chi_p$ of $F_2$PNNNO takes a maximum at around 18 K and below this temperature, $\chi_p$ values go exponentially to zero as the temperature decreases. [Fig. 11(a)] The magnetization isotherm at 0.5 K is shown in Fig. 11(b). The magnetization saturates with two steps. The finite magnetization is not observed below 9 T, above which it begins to grow. In the field region of 15–25 T, the magnetization takes half the value of the saturation magnetization. Above 25 T, it again increases and reaches a saturation at 29 T. The saturation magnetization value corresponds to the parallel alignment of 1 mol of $S=1$ spins. The two-fold saturation of the magnetization process in $F_2$PNNNO contrasts with the linear increase of the magnetization of PNNNO in spite of the fact that these two compounds have the similar structures (described in the preceding section).

Here, we discuss the magnetization isotherm of the type-I chain shown in Fig. 2(a). In the extreme limit of $J_F\rightarrow\infty$, the type-I chain becomes $S=1$ antiferromagnetic uniform chain. Numerical calculations for the $S=1$ antiferromagnetic chain[13] reveal that no plateau appears in the magnetization isotherm. In the other limit of $J_F\rightarrow 0$, the type-I chain is reduced to the combination of $S=1/2$ antiferromagnetic uniform chain and isolated $S=1/2$ spins. The $S=1/2$ antiferromagnetic uniform chain is Bethe-anzatz soluble and the ground state was exactly elucidated. Thus, in this limit no plateau also appears. Since the type-I chain exhibits no plateau in these two extreme limits, it is reasonable to refer that the type-I chain with an intermediate value of $J_F$ is also expected to have no plateau in the magnetization process from the interpolation of two extreme. The observed plateau in $F_2$PNNNO must come from the existence of interchain interactions. In fact, the crystal structure suggests the existence of interchain interactions.

For the description of the magnetization isotherm of $F_2$PNNNO, we define the critical fields of $B_{c0}$, $B_{c1}$, $B_{c2}$, and $B_{sat}$. [Fig. 11(c)] The magnetization is zero below $B_{c0}$, and the beginning and the end of the plateau is represented by $B_{c1}$ and $B_{c2}$, respectively. $B_{sat}$ is the saturation field where the magnetization reaches the full saturation magnetization.

The minimum size of the spin system that yields a plateau in the magnetization isotherm is a 4-spin system of $S=1/2$. The magnetic model of $F_2$PNNNO shown in Fig. 2(b) has

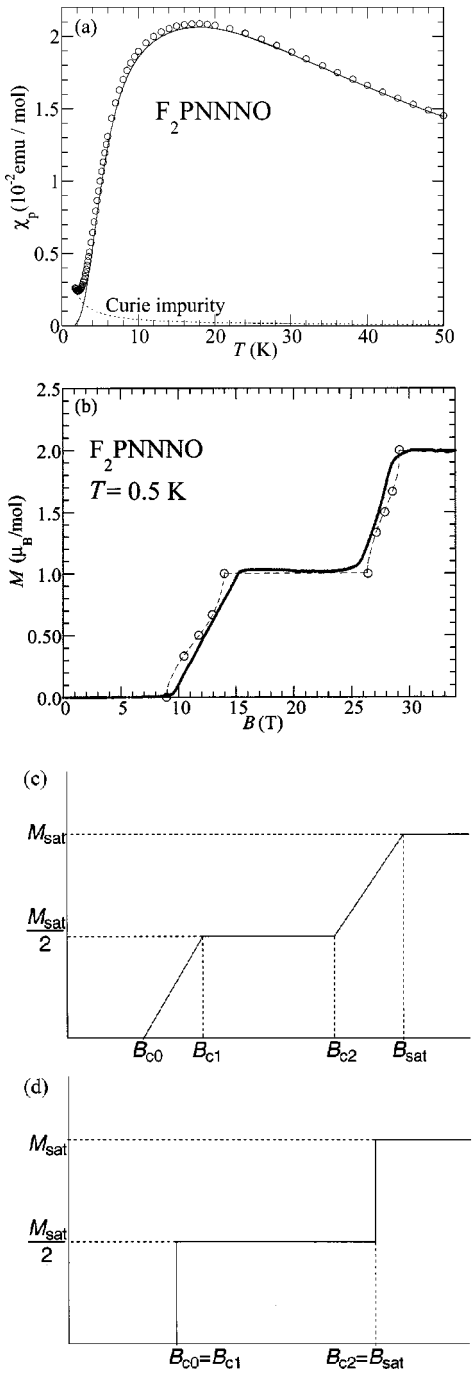


FIG. 11. (a) Temperature dependence of $\chi_p$ of $F_2$PNNNO. Solid curve represents the data after the subtraction of the Curie impurity, which corresponds to 12 mmol of $S=1/2$ species (broken curve). (b) Magnetization isotherm of $F_2$PNNNO at 0.5 K. Open circles represent the calculated results based on the Hamiltonian (6.3) with $\delta=0.8$, $j=-11$, and $2J_{k_B}=-37$ K, which corresponds to $2J_F/k_B=407$ K, $2J'_{AF}/k_B=-67$ K, and $2J_{AF}/k_B=-7.4$ K in Fig. 2(b). (c) Definition of the critical fields and schematic illustration of the magnetization with a plateau of half the value of the saturation magnetization. (d) Schematic display of the magnetization expected for the isolated 4-spin model shown in Fig. 2(c) at $T=0$.

two kinds of antiferromagnetic exchange couplings of $J_{AF}$ and $J'_{AF}$ as intra- and interchain exchange couplings. The interatomic distances suggest that $J'_{AF}$ is larger than $J_{AF}$. Therefore, as a starting point for the understanding, we pick

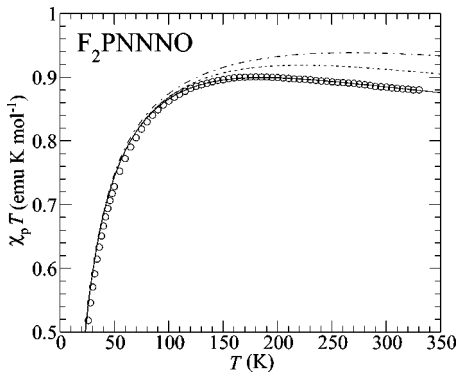


FIG. 12. Temperature dependence of $\chi_p T$ of $F_2$PNNNO. Solid curve is the calculation based on the Hamiltonian (6.3) with $\delta=0.8$, $j=-11$, and $2J/k_B=-37$ K, which corresponds to $2J_F/k_B=407$ K, $2J'_{AF}/k_B=-67$ K, and $2J_{AF}/k_B=-7.4$ K in Fig. 2(b). Broken curve is the calculation for $\delta=0.8$, $j=-15$, and $2J/k_B=-37.5$ K, which corresponds to $2J_F/k_B=562.5$ K, $2J'_{AF}/k_B=-67.5$ K, and $2J_{AF}/k_B=-7.5$ K in Fig. 2(b). Dot broken curve is the calculation for an isolated 4-spin model shown in Fig. 2(c) with $2J_F/k_B=790$ K and $2J'_{AF}/k_B=-71.2$ K.

up a 4-spin system shown in $S=1/2$ [Fig. 2(c)] to examine $J'_{AF}$. The 4-spin model of Fig. 2(c) shows a two-step saturation process with a plateau of half the value of the saturation magnetization. [Fig. 11(d)] In the extreme limit of $J_F\rightarrow\infty$, the system is identical to an isolated dimer model of $S=1$, and the following relation is retained at $T=0$: $B_{c0}/B_{sat}=0.5$. For $J_F\rightarrow 0$, $B_{c0}$ becomes zero. In the case of $0<J_F<\infty$, the magnetization process with two-step saturation is expected. At $T=0$, $B_{c0}=B_{c1}$, and $B_{c2}=B_{sat}$, the critical fields can be written as a function of $x=|J_F/J'_{AF}|$,

$$B_{c0(T=0)}/|2J'_{AF}|=[(1+2x+4x^2)^{1/2}-x-(1+x^2)^{1/2}]/2 \tag{6.1}$$

$$B_{sat(T=0)}/|2J'_{AF}|=[1-x+(1+x^2)^{1/2}]/2. \tag{6.2}$$

Since our experiment was done at 0.5 K, the critical fields of $B_{c0}$ ($=B_{c1}$) and $B_{sat}$ ($=B_{c2}$) in $F_2$PNNNO are approximated to the fields that give the magnetization values of $M_{sat}/4$ and $3M_{sat}/4$, respectively. In this case, $B_{c0}/B_{sat}=12.5/27.7\simeq 0.451\neq 0.5$. Then we can obtain the exchange couplings of $2J'_{AF}/k_B=-71.2$ K and $2J_F/k_B=790$ K. However, the value of $2J_F/k_B=790$ K is too large to explain the temperature dependence of $\chi_p T$ above 100 K (Fig. 12). As $T$ decreases, the value of $\chi_p T$ of $F_2$PNNNO increases starting from the value of 0.88 emu K mol$^{-1}$ for 320 K and reaches a maximum at around 150 K. Below this temperature, $\chi_p T$ decreases. The $\chi_p T$ behavior above 100 K is mainly governed by the magnitude of $J_F$. In the case of $2J_F/k_B=790$ K, the room temperature value of $\chi_p T$ should be about 1 emu K mol$^{-1}$, which corresponds to the formation of 1 mol of $S=1$ species. The 4-spin model with $2J_F/k_B=790$ K and $2J'_{AF}/k_B=-71.2$ K cannot reproduce the $\chi_p T$ versus $T$ behavior. This disagreement comes from the elimination of the antiferromagnetic contribution $J_{AF}$ in the system of $F_2$PNNNO in the isolated 4-spin cluster model. We must take $J_{AF}$ into consideration to explain the observed magnetic properties. The analysis of the two-dimensional lattice shown in Fig. 2(b) is desired. However, the exact treat-

ment of the model with infinite size is difficult. Then we make an approximation by an infinite system with taking $J_{AF}$ into account as much as possible.

In the extreme limit of $J_F \to \infty$, the model of Fig. 2(b) is reduced to a honeycomb lattice of $S=1$. [Fig. 2(d)] In the case of $J_{AF} \ll J'_{AF}$, the model can be approximated by a cluster inside the loop shown in Fig. 2(d). This cluster is an alternating chain of $S=1$. Note that all the $J'_{AF}$ is correctly taken into account. The half of the $J_{AF}$ is also taken into consideration. The system is still infinite in one direction at least. The numerical study of the magnetization of $S=1$ antiferromagnetic alternating chain for various alternating ratio has already been reported. The calculated magnetization process indicates the plateau at the half value of the saturation magnetization.[14] Recently, experimental study of this system was done and a plateau was observed.[15] The values of the critical fields are listed in Table VI of Ref. 14 for various $\delta$, where $J_{AF}/J'_{AF}=(1-\delta)/(1+\delta)$. From Fig. 11(b), the critical fields of $F_2$PNNNO are estimated to be $B_{c0}=9.5$ T, $B_{c1}=15.4$ T, $B_{c2}=25.8$ T, $B_{sat}=29.0$ T. The comparison of these data to the ones listed in Table VI (a) in Ref. 14, gives the approximate value of $\delta$ to be 0.8.

Next, we perform the numerical calculation of the magnetization for $F_2$PNNNO. We consider a cluster inside the loop shown in Fig. 2(b). The Heisenberg Hamiltonian for the model is written as follows:

$$\mathcal{H}=-2J\sum_{i}^{N/4}\,[-j(\boldsymbol{S}_{4i-3}\cdot\boldsymbol{S}_{4i-2}+\boldsymbol{S}_{4i-1}\cdot\boldsymbol{S}_{4i}) +(1-\delta)\boldsymbol{S}_{4i-2}\cdot\boldsymbol{S}_{4i-1}+(1+\delta)\boldsymbol{S}_{4i}\cdot\boldsymbol{S}_{4i+1}], \quad (6.3)$$

where $S$ denote the $S=1/2$ spin operator and $N$ is the number of sites so that $N/4$ is an integer. We define $J<0$ and $j,\delta>0$. Thus the parameters in Fig. 2(b) are represented by $J_F=jJ$, $J_{AF}=(1-\delta)J$, $J'_{AF}=(1+\delta)J$. This Hamiltonian was recently studied and ground-state phase diagram was reported.[16,17]

For the estimation of the magnetization process at $T=0$, we calculate the lowest energy of the subspace $\Sigma_j S_j^z$ under the periodic conditions for length up to $N=24$ by the Lanczos method and extrapolate the finite size data to the thermodynamic limit using the method introduced by Sakai and Takahashi.[13] That is, Shanks' transformation for the estimation of $B_{c0}$, $B_{c1}$, and $B_{c2}$, and finite size behavior predicted by the conformal field theory for the saturation process are employed.[18]

For the calculation of the temperature dependence of the susceptibilities, we perform exact diagonalization of a chain by the Householder method with increasing length up to 12 spins. Since differences between the susceptibility curves for 12 spins and the ones for 8 spins are indistinguishable within the accuracy of 1% when $k_BT/|J| \geqslant 0.23$, we use the curves for 12 spins as an approximation of the thermodynamic limit $(N \to \infty)$.

We estimated the magnetic couplings to reproduce well both susceptibility and magnetization consistently, and obtained the parameter set of $\delta=0.8$, $j=-11$, and $2J/k_B=-37$ K, i.e., $2J_F/k_B=407$ K, $2J'_{AF}/k_B=-67$ K, and $2J_{AF}/k_B=-7.4$ K. The observed results are compared with the calculation in Fig. 11(b). The magnetization isotherm itself can be slightly better reproduced with the parameter set: $\delta=0.8$, $j=-15$, and $2J/k_B=-37.5$ K, i.e., $2J_F/k_B=562.5$ K, $2J'_{AF}/k_B=-67.5$ K, and $2J_{AF}/k_B=-7.5$ K. However, $j=-15$ is too large to explain the temperature dependence of $\chi_pT$ above 150 K. (Fig. 12) The solid curve in Fig. 12 represents the calculation base on the Hamiltonian (6.3). For the correction of the diamagnetic susceptibility, we use Pascal's law. The ambiguity of the diamagnetic correction can affect the slope of the temperature dependence above 150 K, but does not change the maximum value of $\chi_pT$. For the estimation of $J_F$, it is reliable to use the high-temperature data, since at low temperature such as 0.5 K the behavior is influenced by other small interactions. Moreover, $J_F$ is expected to be almost independent on the temperature, because it is the exchange coupling within a molecule. The influence of the thermal expansion on the intramolecular interaction is expected to be small. Therefore, we think that the value of $2J_F/k_B=407$ K is reliable and conclude the intermolecular interactions are $2J'_{AF}/k_B=-67$ K, and $2J_{AF}/k_B=-7.4$ K.

The observed saturation processes (in the field region of $9\sim15$ T for the first saturation and of $25\sim27$ T for the second one) in Fig. 11 exhibit almost linear field dependence, whereas the calculation indicates the increase of the magnetization with the shape of inverse-$S$-type. The reason for the difference in the experiments and calculation is a feature problem. The linear field dependence is probably reflecting the two-dimensionality of $F_2$PNNNO. $F_2$PNNNO is a rare example having an energy gap and a plateau in the magnetization process among spin systems with dimensions higher than one.

## VII. SUMMARY

Three related organic biradicals PNNNO, $F_2$PNNNO, and PIMNO were synthesized and the magnetic properties are examined by susceptibility and magnetization measurements down to 0.5 K and up to 34 T. The numerical calculations are also done considering the crystal structures. Each biradical involves two spins of $S=1/2$, which couple ferromagnetically. These spin pairs couple antiferromagnetically in the crystal. PNNNO and PIMNO are well understood by one-dimensional antiferromagnetic chain models of ferromagnetic spin pairs. Both compounds undergo Néel orders at 1.1 and 2.5 K, respectively, due to weak interchain interactions. The heat capacity measurements of both compounds reveal the three-dimensional nature of these transitions. On the other hand, $F_2$PNNNO has two kinds of antiferromagnetic interactions and forms a two-dimensional system. The magnetism of $F_2$PNNNO is characterized by the singlet ground state and a plateau in the magnetization isotherm. These properties are quite rare among higher-dimensional spin systems than one-dimensional ones. Our theoretical calculation using an one-dimensional approximation gives a qualitatively good explanation for the observed results.

## ACKNOWLEDGMENTS

This research was supported in part by Grants-in-Aid for Scientific Research No. 10146102 on Priority Areas and No. 09740535 from the Ministry of Education, Science, and Culture, Japan. Support from the Hayashi Foundation of Scientific Research is also acknowledged.

[1] F. D. M. Haldane, Phys. Rev. Lett. **50**, 1153 (1983); Phys. Lett. **93A**, 464 (1983).
[2] Y. Ajiro, T. Goto, and H. Kikuchi, T. Sakakibara, and T. Inami, Phys. Rev. Lett. **63**, 1424 (1989).
[3] K. Hida, Phys. Rev. B **45**, 2207 (1992).
[4] H. Manaka, I. Yamada, and K. Yamaguchi, J. Phys. Soc. Jpn. **66**, 564 (1997).
[5] M. Hagiwara, Y. Narumi, K. Kindo, T. C. Kobayashi, H. Yamakage, K. Amaya, and G. Scumauch, J. Phys. Soc. Jpn. **66**, 1792 (1997).
[6] M. Takahashi, Y. Hosokoshi, H. Nakano, T. Goto, M. Takahashi, and M. Kinoshita, Mol. Cryst. Liq. Cryst. Sci. Technol., Sect. A **306**, 423 (1997).
[7] K. Inoue and H. Iwamura, Angew. Chem. Int. Ed. Engl. **34**, 927 (1995).
[8] Y. Hosokoshi, K. Takizawa, H. Nakano, T. Goto, M. Takahashi, and K. Inoue, J. Magn. Magn. Mater. **177-181**, 634 (1998). This paper briefly describes the susceptibility data of PNNNO, $F_2$PNNNO, and PIMNO. However, the exchange couplings of all the compounds are estimated based on the $S=1/2$ alternating ferro- and antiferromagnetic Heisenberg chain model, which is not valid except for PIMNO.
[9] Y. Hosokoshi, K. Katoh, H. Kumagai, K. Inoue, and H. Iwamura (unpublished).
[10] Y. Hosokoshi, D. Shiomi, M. Tamura, K. Nozawa, N. Iwasawa, H. Aruga Katori, T. Goto, and M. Kinoshita, Physica B **201**, 497 (1994).
[11] J. J. Borrás-Almenar, E. Coronado, J. Curely, R. Georges, and J. C. Gianduzzo, Inorg. Chem. **33**, 5171 (1994).
[12] Y. Nakazawa, M. Tamura, N. Shirakawa, D. Shiomi, M. Takahashi, M. Kinoshita, and M. Ishikawa, Phys. Rev. B **46**, 8906 (1992).
[13] T. Sakai and M. Takahashi, Phys. Rev. B **43**, 13 383 (1991).
[14] T. Tonegawa, T. Nakao, and M. Kaburagi, J. Phys. Soc. Jpn. **65**, 3317 (1996).
[15] Y. Narumi, M. Hagiwara, R. Sato, K. Kindo, H. Nakano, and M. Takahashi, Physica B **246**, 509 (1998).
[16] W. Chen and K. Hida, J. Phys. Soc. Jpn. **67**, 2910 (1998).
[17] W. Chen, K. Hida, and H. Nakano, J. Phys. Soc. Jpn. **68**, 625 (1999).
[18] D. Shanks, J. Math. Phys. **34**, 1 (1955).